

Calibration of a compact XUV soft X-ray monochromator with a digital autocollimator *in situ*

Jih-Young Yuh,* Shang-Wei Lin, Liang-Jen Huang and Long-Life Lee

National Synchrotron Radiation Research Center, 101 Hsin-Ann Road, Hsinchu Science Park, Hsinchu 30076, Taiwan.

*Correspondence e-mail: jyuh@nsrrc.org.tw

Received 9 March 2016

Accepted 14 June 2016

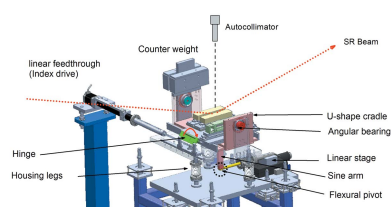
Edited by M. Yamamoto, RIKEN Spring-8 Center, Japan

Keywords: metrological instrumentation; soft X-rays; extreme ultraviolet (EUV); diffraction gratings; autocollimator; on-site beamline diagnostic.

A digital autocollimator of resolution $0.1 \mu\text{rad}$ (0.02 arcsec) serves as a handy correction tool for calibrating the angular uncertainty during angular and lateral movements of gratings inside a monochromator chamber under ultra-high vacuum. The photon energy dispersed from the extreme ultraviolet (XUV) to the soft X-ray region of the synchrotron beamline at the Taiwan Light Source was monitored using molecular ionization spectra at high resolution as energy references that correlate with the fine angular steps during grating rotation. The angular resolution of the scanning mechanism was $<0.3 \mu\text{rad}$, which results in an energy shift of 80 meV at 867 eV . The angular uncertainties caused by the lateral movement during a grating exchange were decreased from $2.2 \mu\text{rad}$ to $0.1 \mu\text{rad}$ after correction. The proposed method provides a simple solution for on-site beamline diagnostics of highly precise multi-axis optical manipulating instruments at synchrotron facilities and in-house laboratories.

1. Introduction

Over the last few decades various accelerator-based synchrotron radiation facilities have provided a greater range of photon sources to fulfill the needs of many research disciplines and industrial applications. For fourth-generation light sources, with basic requirements of high brilliance and small spot size (Eberhard, 2015), more stringent features such as diffraction-limited and coherence preservation have reinforced the performance of new beamlines. In-vacuum monochromators are the most delicate instrument on a beamline. Their high-quality optical elements (mirrors, gratings and crystals) with their precise mechanical adjustment devices should be well characterized (in the laboratory) with apparatus such as Fizeau interferometers, long-trace profilers (LTPs) and nanometer optical measuring machines (NOMs) of in-house metrology laboratories (Yashchuk *et al.*, 2014). After a monochromator is installed on a beamline, deformation of the optical surfaces can be induced by mechanical strain, not to mention the influence of the intense heat load from the synchrotron photons. Both effects severely degrade the beamline performance in terms of resolution and flux density. For observing and quantifying these errors, however, equipment in in-house laboratories becomes difficult to access under ultra-high vacuum environments. At-wavelength metrology has recently been performed at only a few dedicated beamlines at some synchrotron facilities (Schäfers *et al.*, 2016); on-site dynamical monitoring of grating angles during beamline commissioning has been performed (Qian *et al.*, 2009) using a portable long-trace profiler (PLTP) with angular resolution $\pm 2 \mu\text{rad}$ to monitor the grating angle of a monochromator that became degraded due to mechanical failures



after prolonged operation. In this communication we attempted to solve the following problems: (i) a portable LTP might be difficult to install on a regular beamline because of insufficient space or proper inspection viewports; (ii) the energy resolution of the X-ray absorption spectroscopy (XAS) as references are insufficient because of the local chemical bonding and background normalization. Thus, we replaced the PLTP with a commercial autocollimator with accuracy $0.1 \mu\text{rad}$ (0.02 arcsec) and XAS with gas-phase photo-ionization absorption spectroscopy (PAS). Using our home-made monochromator chamber, an ultimate resolving power of better than 10000 at 400 eV was achieved after the accuracy and reproducibility of the scanning mechanism were improved.

2. Apparatus and measurements

Beamline BL08B at the Taiwan Light Source serves multiple purposes (Yuh *et al.*, 2015); the cylindrical-grating monochromator (CGM)-type beamline is one of the mainstream designs in the booming era of synchrotron development (Chen, 1987). The optics layout of the beamline is shown in Fig. 1(a). Two spherical gratings (350 and $1000 \text{ grooves mm}^{-1}$; Horiba Jobin-Yvon) can be chosen separately to cover energy ranges 80 – 420 eV and 350 – 1200 eV , respectively. The monochromator system consists of two exchangeable gratings and a movable exit slit (travel range $\pm 35 \text{ cm}$) to optimize the monochromatic photon energy at variable positions due to the off-Rowland-circle condition. The final beam spot is refocused at a beam quality diagnostic endstation; for details of the beamline design and gas-phase measuring system refer to Yuh *et al.* (2015). Fig. 1(b) presents the CAD design of the monochromator chamber that was modified based on work by Hulbert *et al.* (1990). The synchrotron beam is incident with angle α and diffracted with angle β relative to the normal of the grating surface with $\alpha + \beta$ fixed at 175° (Fig. 1c); the photon energy is selected on rotating the grating to a specific angle φ according to the grating equation (see below). Two gratings were mounted in parallel across the beamline direction on a cradle that accommodates three gratings in total (two currently). The U-shaped cradle in Fig. 1(b) is made of stainless steel with a counterweight at one side to increase the stability and balance. Three gratings with holder on the roller cover plate are seated on the bottom plate of the U-shaped cradle; the cover is also linked to the index drive with a hinge that allows angular and lateral movement (switching of the grating position). Two angular contact bearings tug on the side plate of the cradle and shaft through a

V-groove of the outer housing. The entire weight of the cradle and the housing is due to a pedestal with three legs, each enveloped with a welded bellows from under the housing. This design could effectively damp small vibrations of the vacuum chamber. The position of the vacuum chamber is adjustable with kinematic mounts on girders fixed directly to the ground. The scanning angle of the cradle (grating) is controlled by the sine arm (Fig. 1b), with its upper end connected to the cradle, through a rectangular slot on the bottom plate of the housing; the lower end of the sine arm is joined to the driven rod with a flexible pivot bearing, shown by the dotted circle in Fig. 1(b). With their frictionless and stiction-free design, the bearings have been proven for their precise movement in applications of high-precision small-angle generators in some national metrology institutes (Geckeler *et al.*, 2010). The rod was actuating inside the vacuum chamber (through a welded bellows) driven with a precise linear stage (Micos; UPM-160) from the air. The moving distance is recorded with a linear encoder with overall accuracy and bi-directional repeatability attaining $0.25 \mu\text{m}$ and $0.1 \mu\text{m}$ per scanning 50 mm range, respectively. A theodolite was used to align the height and orthogonality of the optical center relative to the beam position and rotation centers (pitch, yaw and roll) that must be aligned coincidentally with a dual laser-alignment system. The adjustment procedure is described in detail by Tsang *et al.* (1992). In the design of the Dragon-type beamline (Chen, 1987), the grating is the only optical element between the entrance and exit slits; the ultimate resolving power is thus dominated by the performance of the grating. The angular separation of the diffracted light can be derived from the grating equation with oblique incidence,

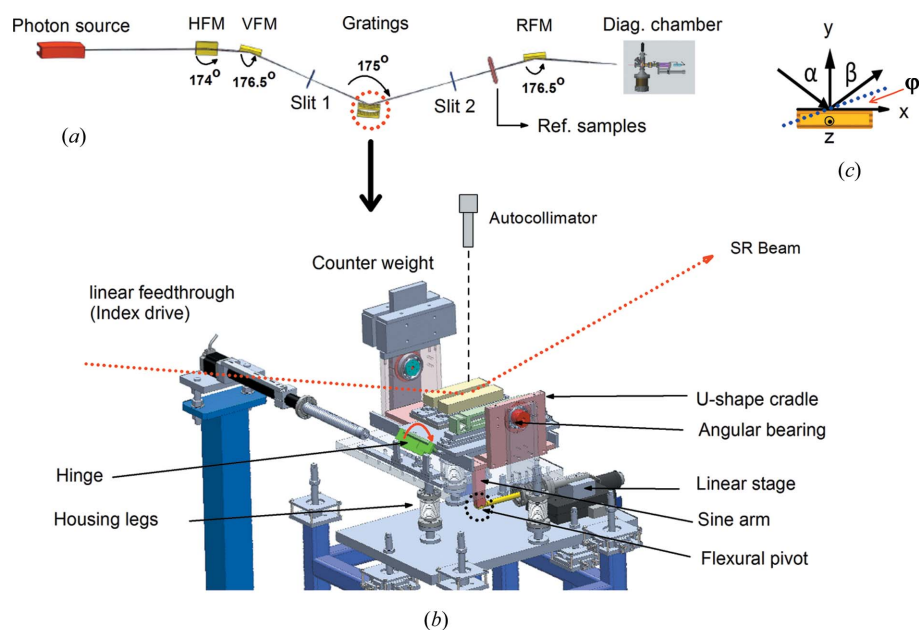


Figure 1 (a) Layout of beamline BL08B. (b) Perspective view of the monochromator chamber (with top flange removed). (c) Incident and diffracted angle of the synchrotron radiation. φ is the grating scanning angle.

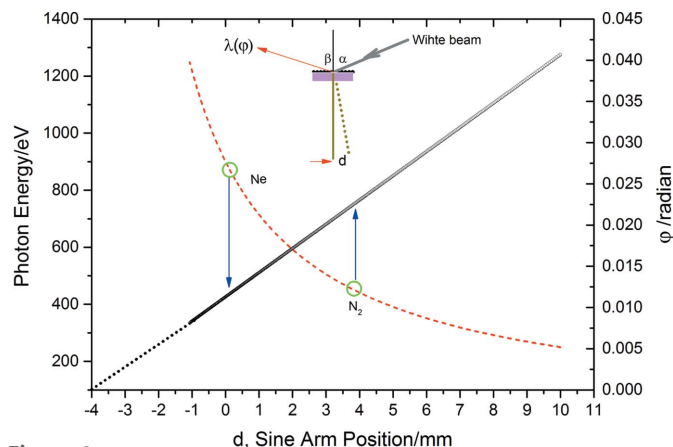


Figure 2 Scanning angle *versus* sine arm position (dark line, right-hand y-axis); photon energy converted with the grating equation (red curve, left-hand y-axis); and energy curve calibrated with gaseous neon and nitrogen photo-ionization absorption spectra.

$$m\lambda = g(\sin \alpha + \sin \beta), \quad \alpha = \varphi + \theta, \quad \beta = \varphi - \theta, \quad (1)$$

$$\varphi = \arcsin[m(hc/E)/2g \cos \theta], \quad (2)$$

in which α and β are the incident and outgoing angles of the photon beam, φ is the grating scanning angle, m is the diffraction order, c is the speed of light, h is Planck's constant, E is the photon energy, g is the ruling width of the grating and 2θ is the included angle of the zeroth-order light (here 175°). The scanning angle is proportional to the moving distance of the sine arm. Fig. 2 illustrates how the photon energy was decoded and connected to an error-free sine arm; with its displacement d recorded with a linear encoder on the scanning stage (to the push-pull sine arm), the scanning angle of the grating can be deduced from $\sin \varphi = d/R$ (dark line, right-hand y-axis in Fig. 2), as the length of the sine arm R is a measured constant. Note that the reference of the horizontal plane (specular reflection) is extrapolated near -4 because of the random selection of the reference point for the encoder. Next, using equation (2), the photon energy at any angle can be calculated from the displacement of the linear stage (red dotted curve, left-hand y-axis in Fig. 2). To verify the validity of this curve, two gaseous samples were chosen at 869 and 401 eV for energy calibration. Any disorientation of the grating caused by an irreproducible mechanical design induces a deviation from the spectral lines, judged from the steep slope of the energy curve in the high-energy region, which indicated larger spectral line separations per unit grating scan. In our estimation,

the dispersion rates per μrad at 1200 eV and 400 eV are 0.16 eV and 0.017 eV, respectively. These results imply that the same mechanical error will amplify the energy uncertainty at high photon energy.

3. Results

To monitor the energy shift, the grating angle should be gauged not only by the displacement of the sine arm but also by a more precise tool for direct and independent measurement of the grating angle. A digital autocollimator is a sensitive instrument for measuring small angular variations of a reflecting surface. Application in industry and metrology for calibration of angular standards becomes more demanding, with respect to, for example, gauge block, polygon and straightness of machine tools. The digital autocollimator was recently applied to SI unit traceability and probing the surface topography of synchrotron optics (Yandayan *et al.*, 2014). The background noise was measured on setting the autocollimator on a granite stand; the resulting RMS of the fixed angle in measurement during 1 h was $0.13 \mu\text{rad}$, comparable with the manufacturer's specifications ($0.1 \mu\text{rad}$). To measure the angular instability of the grating surface inside the vacuum chamber, the autocollimator was mounted vertically above a view port of the monochromator chamber on the air side (see Fig. 1b). The measuring angles were compared with the calculated angles of a sine arm (d/R). Fig. 3(a) shows a stability test between 5 and $11 \mu\text{rad}$; in total 50 cycles were recorded in 42 min. The increments of the linear encoder steps (red line) are compared with the measuring angles of the grating surface

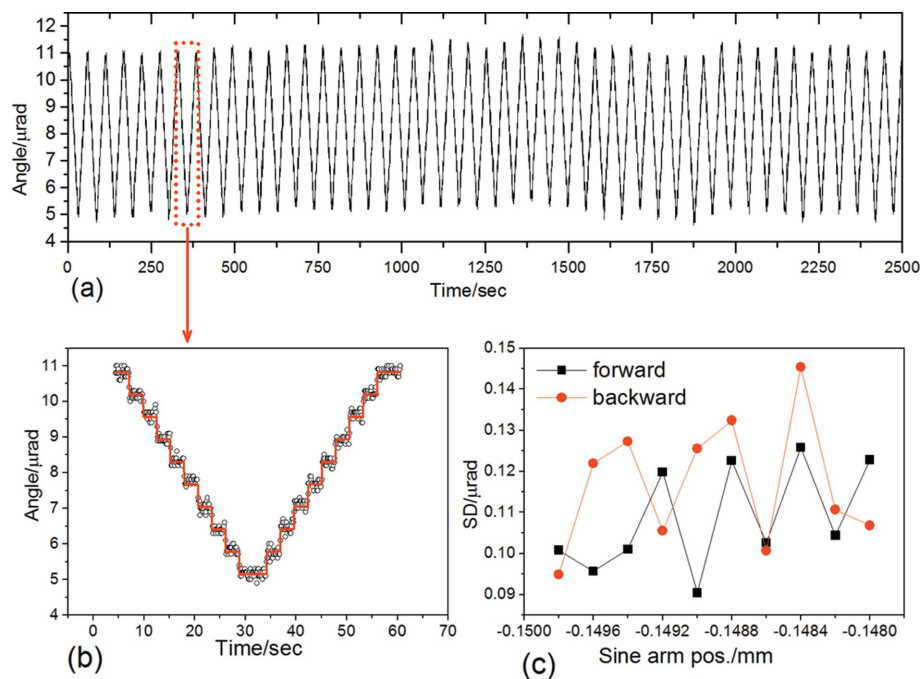


Figure 3 (a) Fine step scan of the grating angle between 5 and $11 \mu\text{rad}$ within 1 h. (b) Zoom of one cycle from (a); the increments of the linear encoder steps (red line) are compared with the measuring angle of the grating surface with the autocollimator (scattered dots). (c) Standard deviation of stability in both directions.

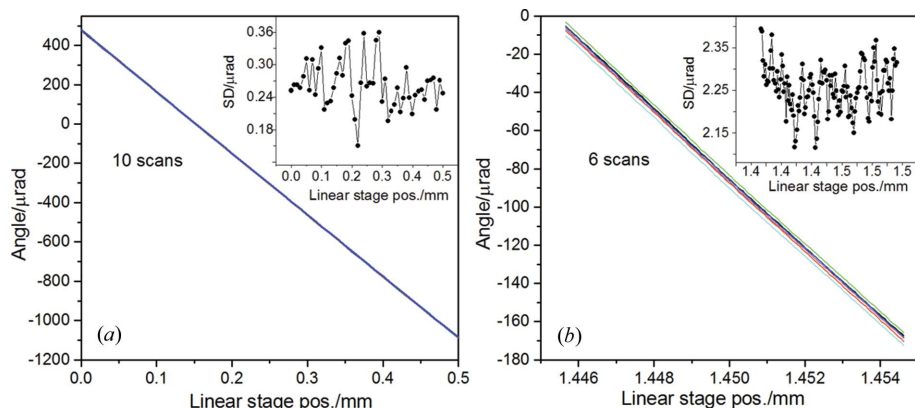


Figure 4

(a) Repeated scans of the grating angle without switching of the grating position; the standard deviation corresponds to the sine arm position (inset). (b) After switching position.

by the autocollimator (scattered dots) in Fig. 3(b). The position of the linear stage remained constant (within elapsed time 5 s); the standard deviation of the measuring angle in Fig. 3(c) again shows reasonable consistency with the specification. The discrepancy indicated errors induced by the mechanical linkage (mostly backlash) in both angular and lateral movements (grating exchange), which might cause misinterpretation in the photon-energy conversion with a sine arm displacement. Fig. 4(a) displays ten measurements lying between 400 and $-1000 \mu\text{rad}$; the angular standard deviations of the sine arm ranged between 0.15 and $0.36 \mu\text{rad}$. In contrast, Fig. 4(b) shows poor reproducibility of the six switching procedures; the angular uncertainty span is $2.2 \mu\text{rad}$ for both gratings. The pronounced errors indicate that the hinge and roller plate design requires further improvement. An essential task in beamline commissioning is to establish the accuracy and reproducibility of the photon energy. Here we applied PAS experiments of four gaseous samples: Kr (91.5 eV), CO (287 eV), N_2 (401 eV) and Ne (867 eV) as physical references of the photon energy between 80 and 1200 eV . Because of their intrinsic physical properties, such as peak width and signal sensitivity (cross section), we chose energies of 400 eV and 867 eV as calibration lines for the $1000 \text{ grooves mm}^{-1}$ grating. The nitrogen K -edge absorption spectra in Fig. 5(f) were fitted with seven vibrational states of a Voigt line-shape

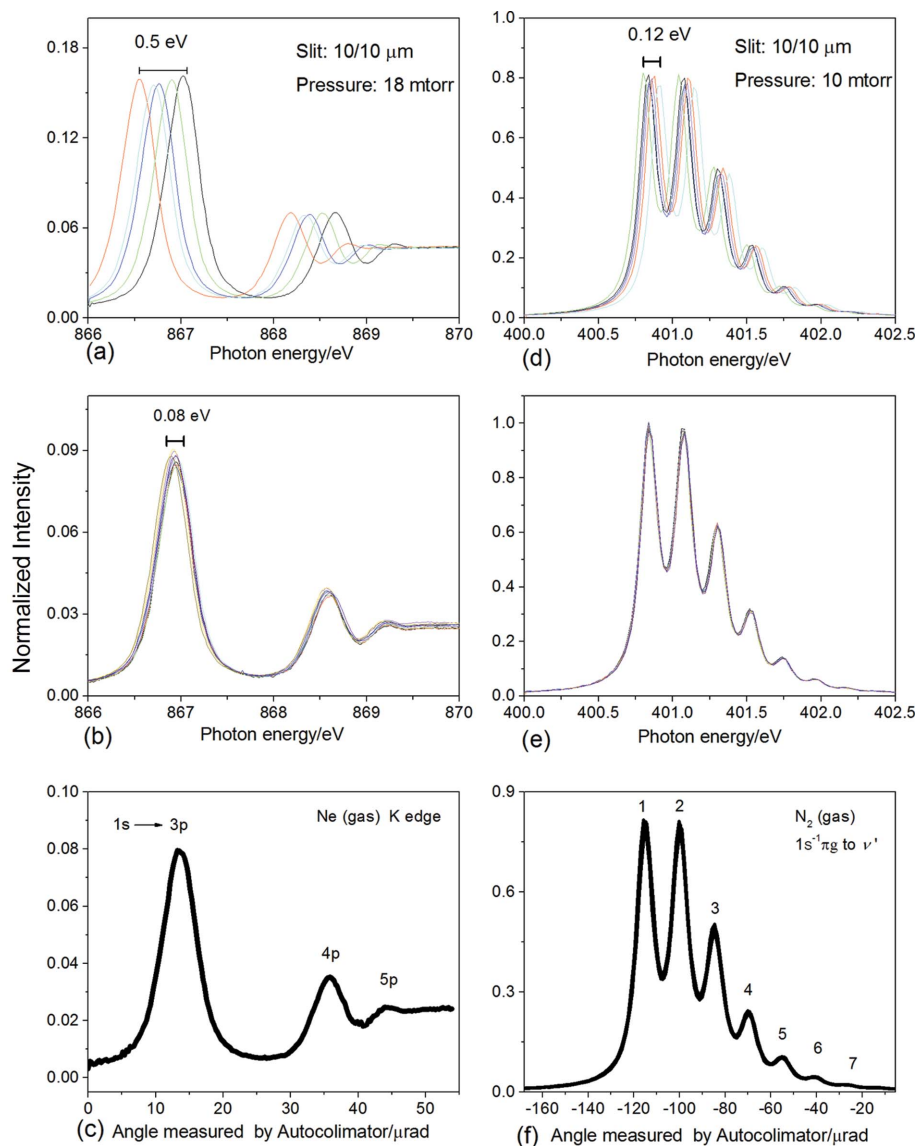


Figure 5

Photon energy of gaseous neon ionization spectra with conversion for the sine arm position. (a) After switching grating position; (b) repeated scans over the same spectral range without switching grating position; (c) repeated scans of the grating angle measured with an autocollimator. (d)–(f) As for (a)–(c) but using gaseous nitrogen; the energy shift was decreased as the angular dispersion is smaller in this range.

function after subtracting a linear background. The fitted results of the FWHM for the Lorentzian and Gaussian shapes of the first line (least photon energy) are 127.6 and 38 meV ; for analysis details see Yuh *et al.* (2015) and Prince *et al.* (1999). Fig. 5(c) displays resonance states for $1s \rightarrow np$ ($n = 3, 4, 5$) of the core excitation of neon, at 867 eV ; with the same analytical method, the Lorentzian and Gaussian widths of states for $1s \rightarrow 3p$, $1s \rightarrow 4p$ are well resolved, and are comparable with results reported by Domke *et al.* (1992). To observe the photon energy

shift under varied grating operating procedures, the gas-phase spectra with energy referenced simultaneously with the sine arm displacement (linear encoder) and grating angle (measured with an autocollimator) are compared in detail. In Fig. 5(a) the neon *K*-edge absorption spectra show a clear energy shift after each switch of the grating position; the energy shift is 0.5 eV, which shows a similar result to that deduced in Fig. 4(b) (from the backlash of the hinge). Fig. 5(b) shows multiple scans in the same spectral range without switching the grating position (only altering the scanning angle); the energy shift is decreased to 0.08 eV. If the photon energy were converted with the angles feedback from the autocollimator as in Fig. 5(c), the photon energy shows satisfactory consistency because the angles misinterpreted by the sine arm were instantly corrected. Figs. 5(d)–5(f) show the same test with gaseous nitrogen; the energy shift after position switching is greatly decreased because the angular dispersion is smaller in this range. Note that the energy reproducibility is acceptable in Figs. 5(c) and 5(f) because here the angular resolution is improved by the autocollimator, *i.e.* 0.1 μ rad.

4. Discussion

The calibration routine is summarized by the block diagram in Fig. 6; first, the actuation movement of the linear stage pushed or pulled the sine arm. The variation of the linear stage position was recorded with the linear encoder and was converted to the rotation angle of the grating. According to equation (1), a specific photon energy was selected. A continuous scan of the grating angles (photon energy) resulted in an ion current because of the gas absorption. An added autocollimator to measure the angle of the grating surface can produce constant feedback and correction in real time. The only drawback is that the working angle of the autocollimator is limited to ± 2000 μ rad; note that the full operational range is from 10 to 40 mrad (equivalent to 80–1200 eV), which means that a long-range measurement would be interrupted. A stitching method should be applied if the entire range of photon energy is to be covered. A partial solution to this problem is to move the grating to a test position (*e.g.* zeroth-order light) to reset the mechanical error after exchanging the grating position, but the process could become tedious during experiments. Alternatively, the autocollimator could be replaced by a wide-angle one (that may sacrifice the resolution) that covers the entire angle of the energy range, which makes the linear stage position for energy conversion become redundant during beamline operation.

In conclusion, we have implemented an on-site beamline diagnostic tool for photon energy to monitor and to correct small angular movements inside a monochromator; the instabilities of photon energy generated by mechanical errors

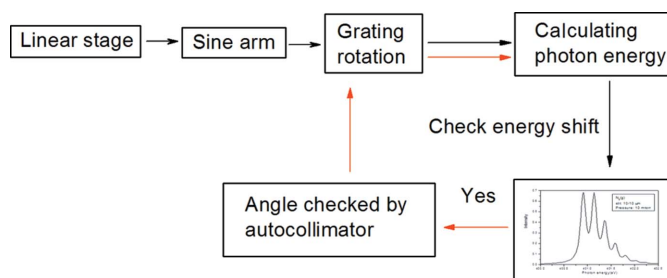


Figure 6
Block diagram of the routine to calibrate the photon energy.

were unveiled by the autocollimator that feeds back the grating angle directly. The pronounced instabilities of photon energy induced by the hinge design are identified and compensated. The method is simple and straightforward, which should be beneficial both for beamline metrology *in situ* and at in-house laboratories.

Acknowledgements

We thank Mr Din-Goa Liu and Mr Shih-Hung Chang for assisting with the installation of the grating chamber, and Mr Te-Hui Lee and Dr Yi-Jr Su for fruitful discussions about the manuscript.

References

- Chen, C. T. (1987). *Nucl. Instrum. Methods Phys. Res. A*, **256**, 595–604.
- Domke, M., Mandel, T., Puschmann, A., Xue, C., Shirley, D. A., Kaindl, G., Petersen, H. & Kuske, P. (1992). *Rev. Sci. Instrum.* **63**, 80.
- Eberhard, W. (2015). *J. Elec. Spectrosc. Rel. Phenom.* **200**, 31–39.
- Geckeler, R. D., Just, A., Krause, M. & Yashchuk, V. V. (2010). *Nucl. Instrum. Methods Phys. Res. A*, **616**, 140–146.
- Hulbert, S. L., Holly, D. J., Middleton, F. H. & Wallace, D. J. (1990). *Nucl. Instrum. Methods Phys. Res. A*, **291**, 343–347.
- Prince, K. C., Vondráček, M., Karvonen, J., Coreno, M., Camilloni, R., Avaldi, L. & de Simone, M. (1999). *J. Electron Spectrosc. Relat. Phenom.* **101–103**, 141–147.
- Qian, S., Arena, D., Dvorak, J. & Qian, K. (2009). *Opt. Eng.* **48**, 113603.
- Schäfers, F., Bischoff, P., Eggenstein, F., Erko, A., Gaupp, A., Künstner, S., Mast, M., Schmidt, J.-S., Senf, F., Siewert, F., Sokolov, A. & Zeschke, T. (2016). *J. Synchrotron Rad.* **23**, 67–77.
- Tsang, K.-L., Tseng, P., Chen, C.-I., Song, Y.-F., Chung, S. C., Dann, T.-E., Lin, H.-F., Huang, L.-R. & Chang, C.-N. (1992). *Rev. Sci. Instrum.* **63**, 1293.
- Yandayan, T., Geckeler, R. D. & Siewert, F. (2014). *Proc. SPIE*, **9206**, 92060F.
- Yashchuk, V. V., Artemiev, N. A., Lacey, I., McKinney, W. R. & Padmore, H. A. (2014). *Proc. SPIE*, **9206**, 92060I.
- Yuh, J.-Y., Lin, S.-W., Huang, L.-J., Fung, H.-S., Lee, L.-L., Chen, Y.-J., Cheng, C.-P., Chin, Y.-Y. & Lin, H.-J. (2015). *J. Synchrotron Rad.* **22**, 1312–1318.